Environmental Science
Processes & Impacts

Diel Mercury Concentration Variations in a Mercury-Impacted Stream

Journal:	*Environmental Science: Processes & Impacts*
Manuscript ID	EM-ART-04-2022-000142.R1
Article Type:	Paper

Environmental Significance Statement

Each component of the mercury (Hg) cycle in stream ecosystems may respond differently to the daily photocycle, across seasons, and influenced by watershed characteristics resulting in complex patterns in observed concentrations. We measured Hg and monomethlymercury (MMHg) concentrations and ancillary water quality parameters over multiple diel cycles in contrasting seasons at several locations along a Hg contaminated creek. Portions of the Hg cycle underwent rapid oscillations correlated with the daily photocycle (sometimes negatively) and were consistent within seasons and opposite in contrasting seasons. Macro-biotic (bioturbation), microbiological (methylation), and abiotic factors exerted control on the observed patterns. The results provide new insights into Hg cycling in contaminated stream ecosystems with potential implications for biotic receptors, monitoring, and remediation.

Diel Mercury Concentration Variations in a Mercury-Impacted Stream

Scott C. Brooks*, Ami L. Riscassi[2], Carrie L. Miller[3], Kenneth A. Lowe, Xiangping Yin, Tonia L. Mehlhorn

Oak Ridge National Laboratory
Environmental Sciences Division
PO Box 2008, MS 6038
Oak Ridge, TN, 37831-6038 USA

[2]University of Virginia, Environmental Sciences Department, 291 McCormick Rd., Charlottesville, VA, USA
[3]Theoretical and Applied Science, Ramapo College of New Jersey, Mahwah, New Jersey, USA

*Corresponding author: brookssc@ornl.gov

ABSTRACT

Filtered and particulate mercury (Hg) and methylmercury (MMHg), and associated water chemistry parameters, were evaluated bi-hourly for several 30-hr periods during the summer and winter seasons at several distinct locations (downstream forested, midstream urban/suburban, upstream industrial) along a creek contaminated with high levels of inorganic Hg to determine if biogeochemical Hg and MMHg cycles respond to the daily photocycle. In summer particulate Hg and MMHg concentrations doubled overnight (excluding the upstream industrial site) concurrent with increases in turbidity and total suspended sediment; no such pattern was evident in winter. Seasonal and diel changes in the activity of macrobiota affecting the suspension of contaminated sediments are likely responsible for these patterns as other potential explanatory variables (e.g., instrument drift, pH, discharge) could not account for the range and timing of our observations. Diel patterns in filtered Hg (Hg_D) were significant only at locations and times of the year when channel shading was not present and daytime concentrations increased 22-89% above nighttime minima likely caused by direct and indirect photochemical reactions. Relationships between Hg_D and dissolved organic carbon (DOC) concentration or character were inconsistent between sites. Unlike Hg_D, there were significant diel patterns in filtered MMHg ($MMHg_D$) at all sites and times of year, with summer concentrations peaking in mid to late afternoon while the timing differed in winter, with concentrations peaking after sunset. Daily variability in $MMHg_D$ concentration ranged between 25-75%. The results imply key controls on net methylation occur within the stream or on the stream bed and include factors such as small-scale temperature changes in the water column and photosynthetic activity of stream biofilm. With respect to stream monitoring, results from this study indicate 1) consistent timing in stream Hg and MMHg sampling is required for accurate assessment of long-term trends, 2) *in situ* measurements of turbidity can be used to quantify diel dynamics of both particulate Hg and MMHg concentrations, and 3) *in situ* fluorescing dissolved organic matter (FDOM), a potential proxy for DOC, was not capable of resolving diel dynamics of filtered Hg or MMHg.

1. INTRODUCTION

Diel biogeochemical processes, including photosynthesis and respiration, flow variation, photochemical reactions, adsorption, desorption, and mineral precipitation and resultant chemical patterns in aquatic ecosystems, including those of dominant and trace anions and contaminants, have been reported in the literature for some time[1-8]. Many of these reports have focused on lentic ecosystems with fewer studies conducted in lotic ecosystems. The physical setting and characteristics of streams and rivers (e.g., unidirectional turbulent flow, varying degrees of canopy cover, longitudinal variation in width to depth ratio) differ significantly from wetlands and lakes making it unclear which lessons from the latter will apply to the former particularly with respect to monomethylmercury (MMHg) concentration dynamics.

Mercury (Hg) is a pollutant of global, regional, and local concern. In aquatic systems Hg can be methylated by microorganisms creating MMHg which is much more toxic and bioaccumulative than its non-methylated form. Hg has a complex cycle in aquatic environments where it is subject to a suite of abiotic (e.g., sorption-desorption, complexation, precipitation-dissolution), photochemical (photo-reduction and -oxidation), and microbially mediated reactions (methylation-demethylation, reduction, and oxidation). Each of these reaction paths may have a unique sensitivity (in direction and extent) and temporal response to the daily photocycle and co-occurring physical and chemical diel patterns. The cumulative impact of these reactions could result from individual components of Hg (dissolved and particulate fractions and different species) exhibiting unique diel patterns that could change throughout the year or between locations with different chemical, physical, and land use characteristics.

A few studies have specifically addressed daily patterns in total and filtered MMHg ($MMHg_T$ and $MMHg_D$, respectively) concentrations in aquatic systems, with the majority located in lakes or wetlands. Observed patterns have been inconsistent for both types of systems, indicating a host of variables may have a role in determining the resultant diel patterns. In a border wetland to the Great Salt Lake, $MMHg_D$ concentration declined during the day and increased at night [4]. The authors attributed the decline in MMHg during the day to photo-demethylation while the increase at night was believed to be due to turnover of thermally stratified water that was below the zone of photodemethylation. In contrast, MMHg concentrations increased during the day, correlated with solar radiation, in two lakes evaluated by Siciliano et al. [9]. The field observations and the results of *in situ* bottle incubations led the authors to conclude that photoproduction of MMHg was occurring and was dependent on the structure and concentration of DOM in the lakes. Differing diel patterns have been observed in wetlands, MMHg concentrations doubled at night relative to daytime in an agricultural wetland planted with wild rice but did not change over a daily cycle in an adjacent plot planted with white rice suggesting other differences in ambient aquatic biogeochemical properties (e.g., DOM structure, microbial community differences between crops) can moderate the influence of photodegradation on the net MMHg budget [5]. In contrast to the prior wetland study, Krabbenhoft et al. [10] , reported diel trends in MMHg in the Everglades but determined they were not correlated to the photocycle; no hypothesis was provided for the patterns. In addition to field studies, consistent findings in bottle incubation studies that have illustrated a link between MMHg photodegradation and light intensity [11, 12] providing support for the hypothesis that photo-demethylation processes are likely to influence field concentrations but the variety of diel concentration trends illustrate other processes may be more dominant in some systems.

Nimick et al. [13], the only study to evaluate MMHg dynamics in a stream, reported increasing $MMHg_D$ concentrations during the day, peaking in early afternoon with overnight concentration minima, and suggested patterns were likely driven by sunlight and temperature driven methylation. Due to a lack of measurements in any other stream systems, the prevalence and/or consistency of this pattern and dominating processes are unknown.

Evaluations of diel patterns of unfiltered and dissolved Hg are rare in any aquatic system. Krabbenhoft et al. [10], working in the Florida Everglades, reported reproducible diel cycles in unfiltered Hg concentrations and its components, dissolved gaseous Hg (DGM; Hg^0) and reactive Hg (i.e., $SnCl_2$ reducible). All Hg fractions were linked to the daily photocycle, increasing during the day, and the pattern was attributed to photolysis of chromophores on the surface of a solid substrate (e.g., the periphyton mat) giving rise to destabilization of sorbed mercury and net desorption during daylight. Nimick et al. [13], is the first and only other study to evaluate diel unfiltered Hg and Hg_D dynamics in stream systems. In a study of two streams affected by mining and geothermal discharge, they found distinct dynamics with one site having no diel patterns and one having increased daytime concentrations of unfiltered Hg and decreasing daytime concentrations of Hg_D. Hg increases tracked suspended sediment, and the pattern of Hg_D concentrations were attributed to either adsorption-desorption of Hg^{2+} or reduction of Hg(II) to Hg^0 and subsequent evasion of Hg^0. The prevalence and/or consistency of these patterns and dominating processes in stream systems are unknown.

The inconsistent findings from lake and wetland studies and lack of studies in streams, with respect to diel variability in Hg and MMHg, illustrate a knowledge deficit of the dominant controls and resultant patterns tied to the daily photocycle. Furthermore, the diel evaluations that have been conducted have focused on a single location or time of year and were not evaluated within the context of Hg dynamics that occur over longer time periods (monthly/annual).

Our objectives for this study conducted in a well characterized Hg-impacted stream were to (i) quantify diel patterns of particulate and dissolved Hg and MMHg and associated water quality parameters at one site in distinct seasons (winter and summer), at multiple sites in the same season (summer), and over several years at the same site in the same season, (ii) determine if diel patterns in Hg and/or MMHg fractions are present at distinct locations and times of year, and if they are related to the daily photocycle, (iii) evaluate the relationship between any observed diel patterns in particulate and dissolved Hg and/or MMHg to water quality parameters, specifically those associated with co-transport (e.g., total suspended solids (TSS), DOC). We also evaluate the potential for *in situ* measurements of turbidity and Fluorescing Dissolved Organic Matter (FDOM) to be used as surrogates for TSS and particulate Hg and MMHg and

DOC and dissolved Hg and MMHg, respectively. These analyses will be used to gain insight into the likely mechanisms responsible for observed diel variability of Hg and MMHg in this stream ecosystem and quantify the importance of processes that operate on a short-term timeframe relative to long-term annual variability.

2. METHODS

2.1 SITE DESCRIPTION

East Fork Poplar Creek (EFPC) is a fourth-order stream in the Valley and Ridge Province of the southern Appalachians in eastern Tennessee, USA. EFPC has been heavily studied and many detailed summaries of its history and characteristics can be found in the literature [14-17]. The creek and surrounding environs were contaminated with Hg due to activities at the Y-12 National Security Complex located at the creek headwaters. The climate is humid subtropical with mean annual temperature 14.5°C and precipitation evenly distributed through the year (mean annual ~137 cm) [18]. Streamflow can exhibit strong seasonality due to high rates of evapotranspiration in summer [18, 19]. During winter there is no canopy cover although there are localized areas of heavy shading due to high, steep creek banks and as the creek flows at base of the north facing slopes of prominent ridges. During summer heavy canopy cover shades much of the creek channel. From its headwaters, the creek meanders 26 km through commercial, residential, open-land and woodland sections of the city of Oak Ridge, TN to its confluence with Poplar Creek (Figure 1). Our study sites are located 5.4, 16.2 and 23.4 km upstream of the mouth of the creek (hereinafter referred to as EFK 5.4, EFK 16.2, and EFK 23.4; Table S.1). Comparison of aerial photographs taken in February versus June indicates that in summer 18%, >95% and 90% of the channel is covered by canopy at EFK 23.4, EFK 16.2, and EFK 5.4, respectively (Supporting Information). The EFK 5.4 site is 3 km upstream of the confluence with Bear Creek, the major tributary to EFPC making EFPC a third-order stream at our farthest downstream sampling site. The Oak Ridge wastewater treatment facility (ORWTF) discharges treated effluent at EFK 13.5. This effluent is a source of nutrients (nitrate, phosphate), organic carbon, and chloride to EFPC but makes insignificant contributions of Hg and MMHg to the creek. Between 2011-2018 average (s.d.) DOC and $SUVA_{254}$ values of the effluent were 5.5 $mg{\cdot}L^{-1}$ (1.6, n = 51) and 2.4 $L{\cdot}mgC^{-1}{\cdot}m^{-1}$ (0.7, n = 44), respectively, compared to samples collected 300 m upstream of the outfall DOC = 1.9 $mg{\cdot}L^{-1}$ (1.6, n = 32), $SUVA_{254}$ = 2.6 $L{\cdot}mgC^{-1}{\cdot}m^{-1}$ (0.8, n = 29) and 80 m downstream of the outfall, approximately 8-10 creek widths, DOC = 3.0 $mg{\cdot}L^{-1}$ (1.3, n = 26), $SUVA_{254}$ = 2.5 $L{\cdot}mgC^{-1}{\cdot}m^{-1}$ (0.7, n = 26). Scheduled backwash operations and variable influent result in lower overnight effluent discharge rates but only mean daily discharge data are available. Based on rating curves developed at EFK 16.2 and EFK 5.4, we estimated the mean transit time from EFK 23.4 to EFK 16.2 to be ≥ 28 hours, from EFK 16.2 to EFK 5.4 to be ~24 hours, and from the ORWTF outfall to EFK 5.4 to be ~9 hours.

2.2 FIELD METHODS

Most of the field work described in this paper occurred between 28 August 2013 and 18 September 2015. All times given are eastern standard time (EST = UTC – 5:00) using a 24-hour clock. Three diel sampling cycles were conducted under baseflow conditions. Two were conducted in summer (Su2013 = 28-29 August 2013; Su2015 = 17-18 September 2015) and one in winter (W2014 = 10-11 February 2014). During the Su2013 and W2014 campaigns samples were collected at EFK 5.4 to evaluate distinctions between seasons. For the Su2015 campaign samples were collected at EFK 5.4 (forested), EFK 16.2 (urban/suburban), and EFK 23.4 (industrial) to evaluate commonalities and differences at multiple locations within the same channel. During each campaign, samples were collected every 2 hours for 30 hours beginning at 0900 h on the first day and continuing until 1500 h on the following day. Samples were collected using a combination of manually sampling into a new 250 ml glycol-modified polyethylene terephthalate (PETG) bottle or automated sampling with a Teledyne ISCO® sampler (typically overnight periods) retrofitted with a strainer and sample tubing made from Teflon® and collected into Isco ProPak™ disposable sample bags made of low-density polyethylene (LDPE). We previously demonstrated that this autosampling method does not compromise sample integrity for our creek water [20]. Grab samples were collected by wading into the middle of the stream, triple rinsing the bottle with creek water, then filling and sealing the bottle for transport to the lab.

In addition to the diel campaigns described, grab samples were collected at EFK 5.4 each month, twice a day, between the Su2013 and W2014 campaigns to track the timing of the transition between any differences observed in the summer and winter dynamics. During these monthly samplings, one sample was collected in the morning (0800 h -1000 h) and another in the afternoon (1245 h – 1500 h). A final diel campaign of reduced complexity was conducted over a 48-hour period from 14-16 August 2018 (Su2018) at EFK 5.4 in which grab samples were collected from the surface water and from a dedicated push-point probe with a screened interval 30 cm below the sediment-water contact, to evaluate the potential influence of pore water dynamics on stream concentrations. Samples were collected every 3 hours beginning at 0820 h on the first day. During these latter two efforts (monthly sampling from Su2013 to W2014 and Su2018) samples were analyzed for dissolved and total Hg and dissolved and total MMHg only.

Local meteorological data (air temperature, solar radiation) were obtained from a tower located 4.5 km to the southwest of EFK 5.4 (Tower K on the Oak Ridge Reservation; Table S.2). Total diffuse light intensity at sampling sites was measured every 5 minutes using an Onset Inc. HOBO Pendant Temperature/Light Data Logger (model UA-002-64) mounted 1.2 meters above the surface of the water. These instruments have a response range from 0 to 320,000 lux over a wavelength range from 150 to 1200 nm. Photosynthetically active radiation (PAR; $\mu mol \cdot m^{-2} \cdot s^{-1}$ in the wavelength range 400-700 nm) was measured every 15 minutes with a LI-COR Quantum sensor and LI-COR Model LI-1000 data logger. The sensor was mounted 30 centimeters above the water surface near the center of the creek channel. Multiparameter sondes were installed adjacent to the pressure transducer at each site and measured and recorded pH, dissolved oxygen, specific conductivity, turbidity (except at EFK 23.4 for Su2015), water temperature, and fluorescent dissolved organic matter (FDOM; Su2013 and W2014 only) at 15-min intervals. Discharge was measured at 15-minute intervals (i) throughout the entire study at EFK 5.4, and (ii) from spring 2015 throughout the study at EFK 16.2. Discharge for EFK 23.4 at 6-minute intervals was provided courtesy of Y-12 environmental compliance personnel. Details on discharge measurements and calculations are provided in the Supplemental Information.

2.3 SAMPLE HANDLING AND ANALYTICAL METHODS

A list of measured parameters is provided in Table S.2. Immediately after collection, samples were transported from the field site to Oak Ridge National Laboratory (15 min drive). An aliquot of the sample was retained for analysis of unfiltered Hg and MMHg (Hg_T and $MMHg_T$, respectively) and the remaining sample was filtered through either a 0.2 μm analytical filter unit for Hg and MMHg analysis or a 0.2 μm syringe filter (both polyethersulfone (PES) membranes) for dissolved organic carbon (DOC), UV-vis, anion, and cation analysis. Previous work has shown that in EFPC MMHg passing a 0.2 μm filter also passes a 3 kD ultrafilter [21]. Samples collected for total suspended solids (TSS) and particulate organic carbon (POC) analysis were filtered through a tared and pre-baked Whatman GFF glass fiber filter with a 0.7 μm particle retention and dried in an oven at 100°C to a constant weight. Unfiltered and filtered Hg and MMHg samples were preserved to 0.5% (v/v) HCl and DOC samples were preserved to 0.1% (v/v) HCl. Trace metal grade HCl was used for sample preservation. Samples for cation analysis were preserved to 0.5% (v/v) HNO_3 (trace metal grade). Filtered samples for anion and nutrient analysis were held in new PETG or polyethylene containers. All samples were refrigerated at 4°C or frozen (ammonium and soluble reactive phosphorous (SRP)) in the dark until subsequent analysis. Filtered Hg and MMHg samples are herein referred to as dissolved Hg (Hg_D) and MMHg ($MMHg_D$).

Analysis of Hg samples was conducted using a Hg purge and trap system (Brooks Rand MERX). Bromine monochloride was added to all Hg samples a minimum of 24 h before analysis. Hydroxylamine and stannous chloride were added to the samples and the Hg^0 produced was purged from solution and trapped onto gold-coated sand analytical traps [22]. The traps were subsequently heated to release the Hg which was detected by the Cold Vapor Atomic Fluorescence Spectrophotometer (CVAFS). Ambient MMHg was analyzed using modifications of EPA method 1630 [23] which involves the distillation of the water sample followed by ethylation, purge and trap onto Tenax traps, gas chromatographic separation of the Hg species and detection by ICP-MS. This analysis was performed with a Brooks Rand MERX MMHg instrument coupled with a Perkin Elmer Elan-DRC ICP-MS. An internal standard ($MM^{200}Hg$) was added to samples prior to distillation and this isotope was used to quantify MMHg concentrations [24]. Additionally, we verified there was no artifact MMHg formation during processing and analysis of water samples by adding ^{201}Hg to select samples and monitoring the absence of $MM^{201}Hg$. Particulate Hg and MMHg (Hg_P and $MMHg_P$, respectively) were calculated as unfiltered concentration minus dissolved concentration.

DOC concentrations were measured using high-temperature platinum-catalyzed combustion followed by infrared detection of CO_2 (Shimadzu TOC-5000A or Shimadzu TOC-L). UV-visible spectra were collected at 1-nm interval and 0.5 second exposure time from 190-1100 nm wavelength with an HP 8453 spectrophotometer using a 1-cm path length quartz cuvette. Specific ultraviolet absorbance at 254 nm ($SUVA_{254}$), a dissolved organic matter (DOM) composition indicator, was also computed. $SUVA_{254}$ was calculated as the UV absorbance at 254 nm (m^{-1}) divided by the DOC concentration ($mg \cdot L^{-1}$) and reported in units of $L \cdot mg\text{-}C^{-1} \cdot m^{-1}$. Total iron concentrations were generally less than 0.1 $mg \cdot L^{-1}$ and were not high enough to cause significant interference [25].

Dissolved anions (Cl^-, NO_3^-, SO_4^{2-}, PO_4^{3-}) and cations (Na, Mg, Ca, K, Al, Fe, Mn, Sr, Ba, U) were analyzed by ion chromatography (IC) (Dionex DX-120, Sunnyville, CA, USA) and inductively coupled plasma-mass spectrometer (ICP-MS, Perkin–Elmer, Waltham, MA, USA), respectively. POC was determined by measuring the percent of carbon released from the total suspended solids sample by dry combustion using an elemental analyzer (LECO-CNS-2000, St. Joseph, MI).

Samples for DGM analysis were collected in 1-liter acid-washed glass bottles. Bottles were triple rinsed with creek water then filled with no headspace, sealed and transported to the lab for immediate processing. Once in the lab, approximately 750 mL of the sample was transferred into a borosilicate glass washing bottle and the water was sparged with Hg-free N_2 for 2 hours at a flow rate of 0.75 $mL \cdot min^{-1}$. The off gas was directed into acidic potassium permanganate traps (0.06 M $KMnO_4$ in 10% H_2SO_4). After sparging was completed, the sample was weighed to determine volume and the $KMnO_4$ traps preserved for subsequent total Hg analysis by cold vapor atomic absorption spectroscopy (CVAAS).

Details on Quality Assurance/Quality Control, calculation of solid-water partitioning coefficients (K_{SW}), and potential outlier detection are provided in Supplemental Information.

2.4 STATISTICS AND COMPUTATIONS

Statistical analyses were conducted in *R* [26]. Potential outliers were identified using modified z-scores (Supplemental Information, Section 4). For all statistical tests, results were considered significant by adopting an *a priori* Type I error rate of 5%. Reported correlations are Spearman's Rank Correlation coefficient (rho), a nonparametric measure of monotonic correlation between two variables. The magnitude of diel concentration variations, expressed as a percentage, was calculated by dividing the range of observed values by the minimum value, excluding potential outliers. Determination of the dependence of concentration on sampling time was made using the coefficient (ξ) introduced by Chatterjee [27] which is very efficient at determining associations that are non-monotonic or oscillating even with noisy data (Supporting Information; Figure S.1). Estimates of ξ were calculated using the R package XICOR [28].

3. RESULTS

3.1 GENERAL CREEK CONDITIONS DURING SAMPLING

Each sampling campaign occurred under generally clear skies five to seven days after the most recent high flow event (Figure S.2). The combination of high and steep creek banks and summer canopy cover limited the light intensity reaching the creek during all but the midday hours. Creek discharge during each sampling campaign was typical of seasonal baseflow conditions (Table S.4; Figure S.3). Lower flow at EFK 5.4 during the Su2015 campaign compared to Su2013 is attributed to drier antecedent conditions. The antecedent precipitation index [29] based on daily rainfall totals was 83.6 mm and 55 mm in 2013 and 2015, respectively. These estimates include a decay function that assigns greater weight to more recent precipitation (period of record begins 1 April 2001). Mean stream discharge during W2014 was higher than during the summer campaigns due to lower evapotranspiration. Discharge from the ORWTF constituted 12.7%, 10.5%, and 15.1% of the mean daily discharge at EFK 5.4 during the Su2013, W2014, and Su2015 campaigns, respectively (Table S.4).

Water temperature increased after sunrise, peaked in late afternoon, and decreased overnight (Figure 2A). Dissolved oxygen (DO) concentration exhibited a diel pattern correlated with the daily photocycle consistent with photosynthesis occurring in the creek (Figure 2B). pH followed a pattern similar to DO in accordance with the canonical relationship between photosynthesis, O_2 production, and CO_2 consumption driving increased pH (Figure 2C). The Su2013 sampling occurred during a trend of decreasing pH (mean daily pH from 26–31 August = 7.74, 7.68, 7.48, 7.26, 7.25, 7.22) during which the relationship between pH and DO was less clear. Temperature, pH, and DO show very strong dependence on sampling time ($\xi > 0.89$) across all sampling campaigns and sites with oscillations correlated to the photocycle (Table S.5). Across sampling campaigns and sites, there was no clear diel pattern in specific conductance.

3.2 MAJOR CATIONS AND ANIONS

The concentrations of the major cations (Ca, Mg, Na, K) and anions (Cl^-, NO_3^-, SO_4^{2-}) generally had low variability and did not have strong temporal dependence in sync with the daily photocycle (Figures S.4 and S.5). Concentration dependence on sampling time (Table S.5) was typically due to monotonic trends rather than cyclic variations. Exceptions to this are seen in the concentration histories for Na, K, Cl^-, and NO_3^- during the Su2015 campaign at EFK 5.4. The concentration of these four constituents declined then rebounded in sync and all these changes occurred during a ten-hour overnight period and thus were disconnected from the daily photocycle.

3.3 PARTICULATE Hg AND MMHg AND ASSOCIATED PARAMETERS (TURBIDITY, TSS, POC)

In the Su2013 and Su2015 campaigns the concentration of particulate Hg and MMHg, expressed on a per volume basis ($Hg_{P.ngL}$ and $MMHg_{P.ngL}$, respectively) increased overnight at EFK 16.2 and EFK 5.4 coincident with overnight increases in turbidity and TSS (Figure 3 and Figure 4) leading to significant ξ values and strong positive correlations between TSS and $Hg_{P.ngL}$ and $MMHg_{P.ngL}$ (Tables S.5 and S.6). Overnight increases in $Hg_{P.ngL}$ and $MMHg_{P.ngL}$ ranged between 73-200% and 105-500%, respectively, relative to daytime minima (potential outliers removed). Overnight increases in TSS and turbidity ranged between 119-194% and 122-495%, respectively. Turbidity was dependent on sampling time during the winter event, but the effect was weak, the estimate of ξ was imprecise (0.18 ± 0.06; Table S.5), and the dependence was a linear decrease rather than a diel oscillation. Similar diel oscillations in $Hg_{P.ngL}$ and $MMHg_{P.ngL}$ were observed in the Su2018 48-hour event although estimates of ξ were not significant (Figure S.6A and D; Table S.5). In contrast, there were no discernible diel patterns in $Hg_{P.ngL}$, $MMHg_{P.ngL}$, or TSS at EFK 23.4 or during the winter sampling at EFK 5.4.

Because of mercury's strong affinity for particles (particulate Hg accounted for 70-88%, 72%, and 41 % of Hg_T at EFK 5.4, EFK 16.2, and EFK 23.4, respectively)[30, 31], we calculated the particulate Hg to TSS ratio expressed in units of $mg \cdot kg^{-1}$ ($Hg_{P.ngL}$:TSS) at each sampling time for each campaign. This ratio remained relatively constant over time in four of the five sets of observations. Sampling time dependence with diel oscillation was seen in Su2013 at EFK 5.4 ($\xi = 0.41$, $p = 2.5\times10^{-3}$; Figure S.7A and C). The sampling time dependence for $Hg_{P.ngL}$:TSS at EFK 5.4 and EFK 16.2 in Su2015 was due to monotonic trends rather than daily oscillations, the effects were weak to moderate and estimates of ξ were imprecise. Compared to Hg_T, a smaller percentage of $MMHg_T$ was particle associated (21-29%, 38%, and 25% of $MMHg_T$ at EFK 5.4, EFK 16.2, and EFK 23.4, respectively). The particulate MMHg, to TSS ratio ($MMHg_{P.ngL}$:TSS) was independent of sampling time for all events (Figure S.7B and D; Table S.5).

More generally, $Hg_{P.ngL}$ was strongly positively correlated with TSS in four of the five cases (Figure S.8A and C, Table S.6), the one exception being Su2015 at EFK 23.4 (rho = -0.0944, p = 0.719). The slopes of the $Hg_{P.ngL}$ versus TSS regression lines were the same for those cases with significant correlation, i.e., there was no evidence for a sampling event × TSS interaction effect (analysis of covariance, $F_{3, 75} = 1.87$, $p = 0.14$). For each 1 $mg \cdot L^{-1}$ increase in TSS, $Hg_{P.ngL}$ increased by 9.3 ± 1.2 $ng \cdot L^{-1}$. Similarly, there was no evidence for a sampling event × TSS interaction effect for the $MMHg_{P.ngL}$ data regardless of the potential outlier value at EFK 16.2 ($F_{2, 53} = 0.783$, $p = 0.46$). For each 1 $mg \cdot L^{-1}$ increase in TSS, $MMHg_{P.ngL}$ increased by 0.017 ± 0.004 $ng \cdot L^{-1}$ (0.0014 ± 0.003 excluding outlier).

Particulate organic carbon (POC, $mg \cdot L^{-1}$) was measured for the Su2013 and W2014 campaigns only and for each the POC showed a diel oscillation pattern similar to that measured for TSS with daytime minima and overnight maxima (Figure S.9A). The POC concentration dependence on sampling time was stronger in summer than winter ($\xi = 0.59 \pm 0.13$ and 0.32 ± 0.13 in summer and winter, respectively; Table S.5). In contrast, the percent organic C on suspended solids (percent OC per mg TSS) was independent of sampling time (Figure S.9B) although values for winter samples (mean ± sd = 6.4 ± 0.8) were significantly higher than those from summer (5.1 ± 0.5; $p = 3.32 \times 10^{-8}$; Welch's two-sample t-test; including potential outlier).

3.4 DISSOLVED Hg AND MMHg AND ASSOCIATED PARAMETERS (DISSOLVED ORGANIC CARBON)

Dissolved Hg (Hg_D) concentration showed diel oscillations at EFK 5.4 in W2014 and EFK 23.4 in Su2015 ($\xi = 0.47 \pm 0.13$, $p = 4.5 \times 10^{-4}$ and 0.53 ± 0.15, $p = 2 \times 10^{-3}$, respectively) in which concentration increased during the day with mid to late afternoon maxima and overnight minima (Figure 5B and E). Dissolved MMHg concentration showed diel oscillation in each campaign. During the summer campaigns at each location $MMHg_D$ concentrations increased during the day with maxima in mid to late afternoon and declined overnight. At EFK 23.4 in Su2015 $MMHg_D$ concentrations were relatively constant during the day and greater than constant nighttime concentrations. Similar diel oscillations were seen in the surface water samples during the 48-hour campaign in Su2018. Dissolved MMHg concentrations in pore water were, on average, 7× higher than in surface water with no apparent diel oscillations (Figures S.6E and F). In contrast, for the winter sampling the highest $MMHg_D$ was measured well after sunset, approximately six hours later than the daytime maxima measured in summer.

For most campaigns and locations, no diel oscillations were seen for DOC concentration or composition as estimated from $SUVA_{254}$ (Figure S.10). However, at EFK 23.4 in Su2015 these two parameters show opposing diel oscillation with DOC increasing during the day and declining overnight whereas $SUVA_{254}$ values were lower during the day and higher at night. FDOM (measured in Su2013 and W2014 only) fluctuated over the sampling period in Su2013 with no apparent diel pattern. A strong diel pattern in FDOM was seen in W2014 with values steadily decreasing during daylight hours and increasing overnight (Figure S.11). The relationship between FDOM and DOC, $SUVA_{254}$, Hg_D, and $MMHg_D$ varied from summer to winter (Table S.8). For example, in Su2013 there were no significant correlations between FDOM and the remaining four parameters regardless of outlier exclusion. In W2014, there was a moderately strong positive correlation between FDOM and DOC and strong to very strong negative correlations between FDOM and $MMHg_D$ and Hg_D. A more extensive data set, spanning multiple seasons and broader range of parameter values would be needed to evaluate more rigorously the potential seasonal and extreme value effects on the use of FDOM as a reliable proxy variable for DOC, Hg_D, and $MMHg_D$. No correlation was observed between FDOM and $SUVA_{254}$ in either Su2013 or W2014 regardless of outlier exclusion.

Because of the reported tight coupling of dissolved Hg and MMHg with DOC [32-34] we examined the Hg_D:DOC and $MMHg_D$:DOC ratio over the course of each sampling campaign. DOC concentrations varied over time but generally did not show diel oscillations. Hg_D concentrations varied over time with diel oscillations in two cases (W2014 at EFK 5.4 and Su2015 at EFK 23.4). $MMHg_D$ concentration varied over time with diel oscillations for all events and locations. Nevertheless, the timing and magnitude of the DOC concentration variations overwhelmed the Hg_D and $MMHg_D$ patterns and significant diel oscillation in Hg_D:DOC was apparent only in W2014 at EFK 5.4 and for $MMHg_D$:DOC in Su2015 at EFK 5.4 (Figure S.12; Table S.5). Additionally, significant positive correlations between DOC and Hg_D were found for only two cases, Su2013 at EFK 5.4 and Su2015 at EFK 23.4 (Table S.7; Figure S.13). Interestingly, these two parameters were strongly negatively correlated in Su2015 at EFK 16.2 (rho = -0.719, $p = 7.67\times10^{-4}$). $MMHg_D$ and DOC were positively correlated only for Su2015 at EFK 23.4 and uncorrelated for all other events and locations.

3.5 DISSOLVED GASEOUS MERCURY (DGM)

Dissolved gaseous mercury concentrations were lower in samples collected in early morning or during night and higher in samples collected in mid-afternoon (Figure 6) with a moderately strong positive correlation between PAR and DGM (rho = 0.47, p = 0.05) using average PAR value for the 2-hour period preceding collection of the DGM sample. Samples for DGM analysis were collected less frequently than for the other analytes precluding meaningful estimation of the ξ statistic.

3.6 TEMPORAL $MMHg_D$ CONCENTRATION PATTERNS IN MORNING VERSUS AFTERNOON SAMPLES

Between the Su2013 and W2014 30-hour sampling campaigns, samples were collected once per month at two different times during the day, once in the morning and again in the afternoon. During summer and early autumn, the $MMHg_D$ concentration was higher in the afternoon than the morning. By mid-autumn there was no difference between samples at different times of day and this lack of difference persisted into winter (Figure 7). These observations are consistent with the February 2014 diel sampling in which there were no differences in $MMHg_D$ concentration for samples collected during daylight.

A summary of the primary results is provided in Table 1. We turn now to a discussion of the results and the mechanisms proposed.

4. DISCUSSION

Because of the estimated travel times between sites (Methods; EFK 23.4 to EFK 16.2 ≥ 28 hours; EFK 16.2 to EFK 5.4 ~24 hours; ORWTF to EFK 5.4 ~9 hours), diel concentration variations at EFK 16.2 likely reflect or integrate reach-scale processes independent of changes observed at EFK 23.4. Similarly, concentration variations at EFK 5.4 were likely independent of changes at EFK 16.2 but were affected by variable discharge from the ORWTF.

4.1 MAJOR IONS

Among the major cations and anions, sodium, potassium, chloride, and nitrate each had a synchronized pattern of concentration dips and recovery during overnight hours at EFK 5.4 in Su2015. As there are no geogenic sources of these solutes in East Fork valley, their presence in EFPC reflects anthropogenic influences. The overnight concentration dynamics are likely the result of decreases in discharge of treated effluent from the ORWTF 8.1 kilometers upstream of our sampling location at EFK 5.4. A similar pattern was not observed for the other sampling campaigns at EFK 5.4 potentially because streamflow was higher and therefore the influence of changes in upstream effluent flow would have a diminished impact on stream concentrations. A long record of sampling this effluent has shown that it is not a source of either Hg or MMHg to EFPC and daily fluctuations in effluent discharge are not expected to affect the diel Hg and MMHg patterns. The dominant ions with geogenic sources in the watershed (calcium, magnesium) showed no similar fluctuations over the sampling periods.

4.2 CONTROLS ON PARTICULATE Hg AND MMHg CONCENTRATIONS, TURBIDITY AND TSS

Over the course of several diel sampling campaigns conducted in summer months, $Hg_{P.ngL}$, $MMHg_{P.ngL}$, and POC concentrations oscillated in sync with corresponding changes in TSS and turbidity at two sites (forested and urban/suburban); these oscillations were counter to the daily photocycle. No such patterns were evident during winter or at the farthest upstream site. In contrast, those summertime patterns in particulate Hg, MMHg, and POC do not appear when normalized to TSS concentration. This suggests that overnight increases in TSS, turbidity, POC, $Hg_{P.ngL}$, and $MMHg_{P.ngL}$ were due to the (re)suspension of the same solids contributing to TSS load during the day and were most likely caused by bioturbation due to the activity of macrobiota in the creek [35-38]. Fine particulate matter export in streams depends on the activity of macroinvertebrates [36]. Higher nocturnal activity has been documented for benthic macroinvertebrates in streams for decades [35]. Studies that have evaluated diel suspended sediment dynamics, including a third-order Pennsylvania piedmont stream [37] and a cobble-bed Montana River [39] both found daytime minimums and nighttime maximums similar in magnitude to this study, from ~3-9 $mg \cdot L^{-1}$ and ~0-3 $mg \cdot L^{-1}$, respectively. Both studies concluded that bioturbation from benthic macroinvertebrates (as well as crayfish, amphibians, and eels in Pennsylvania) was the likely mechanism for increased nighttime concentrations. In the Pennsylvania stream, on average over eleven months, nighttime suspended solids and POC increased by 80% and 43%, respectively, over daytime minima. However, the diel variability was positively correlated with temperature and maximum variability was found in June where nighttime TSS and POC were 155% and 105% greater than daytime values, respectively. One other study assessing diel turbidity[38] found nighttime increases considerably larger than we observed, increasing from close to zero up to 20 $mg \cdot L^{-1}$ at night, however that site was located in an agricultural catchment that included cattle grazing as well as at least five species of bottom dwelling fish. The combination of greater sedimentation from animal induced bank erosion as well as larger and more mobile macrofauna, likely contributed to the relatively elevated nighttime TSS concentrations.

Similarly, in EFPC, the presence and magnitude of the diel turbidity pattern undergoes a seasonal cycle (Figure 8). There are no overnight increases in turbidity in late autumn and during winter. In spring the overnight increases in turbidity return, persist throughout summer, and dampen during autumn until they disappear again. The consistent relationship between turbidity and $Hg_{P.ngL}$ and $MMHg_{P.ngL}$ in seasons with unique diel dynamics indicate that this *in situ* measurement can be used to accurately estimate diel fluctuations in particulate concentration dynamics.

Other potential sources of diel variability in turbidity cannot account for the range of values or timing of our observations. The concordance between turbidity and TSS shows that other diel patterns did not interfere with the turbidity instrument. For example, instrument manufacturers report a temperature dependence of up to -0.6% turbidity per degree Celsius increase. For the temperature range in Su2013 (1.9°C) this accounts for 1.1% variability in instrument reading compared to the 122% observed. Additionally, a similar temperature range occurred in the winter sampling, but no diel turbidity pattern was seen in that season.

Diel patterns in streamflow were not in phase with the turbidity and TSS patterns. For example, at EFK 5.4 during Su2015 a discharge-turbidity hysteresis plot shows turbidity remained constant while discharge varied and changed when discharge was constant (Figure 9). Finally, we cannot account for the turbidity patterns via pH-driven precipitation and dissolution reactions involving carbonate minerals (Figure S.14). The pH decreased overnight, favoring dissolution of carbonate minerals which would decrease turbidity and TSS, which is the opposite of the observed overnight increase. Lack of diel oscillations in calcium and magnesium concentrations also argue against cyclical precipitation-dissolution reactions affecting turbidity and TSS.

Benthic macroinvertebrate taxonomic richness in EFPC is similar to local reference streams for sampling locations near EFK 5.4 and EFK 16.2 whereas it is lower at EFK 23.4 and sites upstream of that location[40]. Similarly, fish communities sampled near EFK 5.4 and EFK 16.2 are similar to local reference stream with respect to population density and the number of pollution-sensitive species[40] suggesting sufficient aquatic fauna in the lower sections of EFPC to cause the diel patterns in TSS and turbidity. The absence of diel patterns in TSS, $Hg_{P.ngL}$, and $MMHg_{P.ngL}$ at EFK 23.4 may be due to one or more reasons. Approximately 25% of the channel upstream of that sampling location is concrete lined with little sediment to be resuspended by fish or benthic invertebrates in addition to being poor habitat for the latter. The benthic macroinvertebrate community upstream of EFK 23.4 is lower density and less rich in pollutant tolerant species compared to downstream locations [40, 41]. Finally, the EFK 23.4 site had the shortest upstream reach (2.6 km) of the three sites so integrates fewer cumulative upstream effects.

4.3 CONTROLS ON DISSOLVED Hg AND MMHg CONCENTRATIONS

The inconsistent relationship between Hg_D, $MMHg_D$, and DOC may be related to the high concentrations of Hg and MMHg in this contaminated stream coupled with the low and narrow range of DOC concentration across seasons and a broad land use gradient in the watershed (industrial, urban/suburban, forested). Dissolved Hg concentrations had diel oscillations at EFK 23.4 in Su2015 and EFK 5.4 in W2014. These correspond to sites and seasons with the least canopy cover. Much of the reach upstream of EFK 23.4 has little to no canopy cover and this site had the largest variation in other sunlight-driven variables (temperature, pH, dissolved O_2). While solar radiation was less intense and the daily photoperiod shorter in the winter sampling, there was no canopy, so sunlight affected a much longer length of the creek upstream of our sampling location than during the summer samplings at EFK 5.4 or EFK 16.2. Photochemical reactions may have promoted the release of particle-bound Hg leading to diel oscillations in Hg_D in sync with the daily photocycle. This may be related to the inferred changes in DOM composition as reflected in the oscillating values of $SUVA_{254}$ and FDOM (Figures S.10 and S.11). Nevertheless, the different FDOM-Hg_D relationship between Su2013 and W2014 demonstrates that additional research is needed before adopting FDOM as a reliable proxy measure for Hg_D. While each parameter may be responsive to the daily photocycle the correlation between them remains unclear. The changing DOC concentration at EFK 23.4 may also play a role in the oscillating Hg_D concentration but the effect of DOC concentration alone is difficult to predict as numerous studies demonstrate that DOM quantity and composition interact to affect Hg solid-water partitioning [42-45].

In addition to the potential for photochemical reactions to directly affect Hg solid-water partitioning, there are indirect light-driven reactions to consider. pH has long been acknowledged as a master variable exerting control on sorption with cation sorption increasing with increasing pH and anion sorption increasing with decreasing pH [46]. In this regard, it is important to consider that we expect all the dissolved Hg to be associated with DOM and that the Hg-DOM complex has a net negative charge at the pH values in EFPC. Equilibrium aqueous speciation calculations indicate that >99% of the dissolved Hg and MMHg would be present as DOM complexes [47] and laboratory experiments show the Hg-DOM association to be kinetically fast [48]. If these assumptions are correct then one would expect the light-driven pH increase during the day to be accompanied by increasing Hg_D concentration, consistent with our observations. In this case, the DOM would be a bridging ligand between surfaces and Hg and the overall Hg partitioning behavior would be dominated by DOM sorption. Generalizations about the sorption of heterogeneous mixtures like DOM are more problematic than for individual ions or molecules. Nevertheless, DOM sorption onto a variety of minerals does seem to consistently decrease with increasing pH and this pH dependence is particularly sensitive in the pH range 6.5-8.5 which encompasses most of our observed range [49, 50]. Therefore, the diel pH oscillations likely contributed to the oscillations in Hg_D concentration at EFK 23.4 and EFK 5.4.

Diel temperature changes can also affect sorption and this effect can be quantified by the reaction enthalpy ($\Delta H°$) using the van't Hoff equation. Still operating under the assumption that the overwhelming majority of Hg_D is present as a Hg-DOM complex the apparent temperature effects on Hg sorption will be dominated by the enthalpy of DOM sorption (also assuming temperature effects on Hg-DOM complexation are negligible). Nguyen [51] reported sorption enthalpies for Elliot Soil humic acid and fulvic acid isolates onto hematite over the temperature range 15-35°C, showing the reactions to be exothermic for both isolates. Using their most extreme enthalpy value ($\Delta H° = -60.7\ kJ \cdot mol^{-1}$) and our broadest diel temperature range (5.54°C, Su2015, EFK 23.4), diel temperature changes are predicted to change the K_{SW} for Hg by 0.2 $\log_{10}$ units (i.e., if $\log_{10}(K_{SW,\ 25°C}) = 6.0\ L \cdot kg^{-1}$, $\log_{10}(K_{SW,\ 19.5°C}) = 6.2\ L \cdot kg^{-1}$). This difference in $\log_{10}(K_{SW})$ is generally smaller than the observed variation (Figure S.15). Therefore, while temperature changes could affect equilibrium Hg sorption, the predicted effect is small and within the range of diel variability.

$MMHg_D$ concentrations showed diel oscillations during each campaign at all locations. Variability in diel $MMHg_D$ concentrations in summer represented 26% - 38% of annual variability over the same period for monthly samples collected at a consistent time of day during baseflow conditions (Figure S.16). Other investigators have reported daytime $MMHg_D$ maxima relative to nighttime minima in lakes, wetlands, and streams when sampled in spring and summer [4, 9, 13, 52]. Dissolved phase MMHg concentrations are subject to some of the same controls that were discussed for Hg_D (photochemical release from surfaces, pH- and temperature-dependent sorption) with the same expected trends and magnitude of effects. Additionally, the measured MMHg concentrations are the net result of the opposing processes of Hg methylation and MMHg demethylation. Under the environmental conditions in this study, Hg methylation is an exclusively biotic process in which MMHg is generated by anaerobic bacteria and Archaea possessing the *hgcAB* two-gene cluster [53, 54]. In contrast, MMHg demethylation can be mediated biotically by a broad array of aerobic and anaerobic microorganisms or by abiotic reactions [12, 55, 56].

Hg methylation within algal biofilms (periphyton) in EFPC is an important process exerting control on the diel oscillations in $MMHg_D$ concentration. Several investigators have reported net positive MMHg generation by algal biofilms [57-65]. Specifically, we have previously documented Hg methylation by EFPC periphyton at several sites in the creek and across seasons [66, 67]. Importantly, MMHg generation by periphyton was significantly slower when biofilms were incubated in the dark or are grown under low light conditions with rates of net MMHg production between light and dark incubations varying by 1120%. In some experiments, biofilm samples incubated in the dark were net demethylating. Once formed inside bacterial cells, MMHg is rapidly exported to the surrounding media and can remain filter-passing for up to 24 hours[68-70]. Rapid MMHg export from the cells coupled with turbulent advective flow in the stream mixes the periphyton-derived MMHg with the water column providing a link between production of MMHg in the periphyton and our observations of $MMHg_D$ concentrations that are positively correlated with the daily photocycle.

Another potentially important source of $MMHg_D$ to surface water is the hyporheic zone. The Su2018 campaign showed that in some locations interstitial porewater can have substantially higher $MMHg_D$

concentration than the surface water (Figure S.6) and relatively small volumes of that water (<10%) could significantly impact surface water concentrations. But the porewater $MMHg_D$ concentrations did not show diel oscillations suggesting either it is a small component of the surface water budget, or another, oscillating, mechanism exerts control on the porewater-surface water exchange. Evapotranspiration (ET) driven oscillations in hyporheic-surface water exchange could have a diel signal in sync with the daily photocycle but the direction of such a signal is the opposite of the observed effect. Increasing ET during the day draws groundwater levels down creating a gradient from surface water to hyporheic and groundwater which is the opposite of that needed to deliver the higher $MMHg_D$ concentration porewater to the surface water. Shorter flow paths disconnected from larger scale groundwater-surface water exchange may be involved but much more detailed hydrogeochemical characterization studies would be needed to test these hypotheses. Additionally, these mechanisms may not transfer to other reaches of the creek where diel $MMHg_D$ oscillations were seen. For example, the reach upstream of EFK 23.4 has few trees to drive the ET oscillations and has long channelized sections with no hyporheic zone.

In addition to these potential sources of $MMHg_D$, an important demethylation mechanism to consider is photodemethylation which has been the subject of intense study in controlled lab settings and field studies [12]. Photodemethylation is a complex multivariate function of chemical (e.g., DOM composition and concentration) and physical (light duration and intensity, water depth) variables presenting significant challenges in generalizing results to our data [71]. In controlled lab studies the rate and extent of $MMHg_D$ photodemethylation were positively correlated to the concentration of an EFPC DOM isolate and was faster and more complete if the DOM was chemically reduced prior to use in experiments [72]. However, photodemethylation would generate diel oscillations opposite to that which was observed. While photodemethylation was likely occurring in our sampling campaigns (particularly at EFK 23.4 in Su2015), the results suggest that the rate of instream Hg methylation was faster than photodemethylation resulting in increasing concentrations during the day that peaked in mid to late afternoon. In W2014, the low water temperatures corresponded to an annual minimum in Hg methylation activity [66, 67, 73] and, given the lack of canopy cover over the creek, photodemethylation may have outpaced Hg methylation resulting in peak $MMHg_D$ concentration after sunset.

4.4 DISSOLVED GASEOUS MERCURY

DGM, sampled only in Su2013 and W2014, showed similar patterns in both seasons and was positively correlated with PAR and it is likely that the diel oscillations were attributable to photochemical reduction of Hg(II) to generate Hg(0). Mid-day maxima and overnight minima in DGM concentration have been reported in all seasons across a broad range of latitudes and correspondingly diverse range of water bodies and chemistries [10, 74-79]. Siciliano et al. [78] reported a diel cycle for DGM in two Canadian lakes with midday maxima and a corresponding cycle in microbial mercuric reductase activity that matched the DGM cycle. Microbial mercury oxidase activity was offset from reductase activity and increased as DGM decreased throughout the afternoon suggesting a role for microbial processes to contribute to abiotic photochemical reactions in modulating DGM concentrations. Hg stable isotope patterns in EFPC suggest that microbial Hg(II) reduction and, to a lesser extent, Hg(II) photoreduction contribute to Hg cycling in the creek [80]. Notably, in the only other sunrise-to-sunset sampling study conducted in a Hg-contaminated creek of which we are aware, DGM concentration peaked in mid-morning and declined throughout the day [81].

5. CONCLUSIONS

Several diel sampling campaigns at multiple locations in EFPC confirm that portions of the Hg cycle in freshwater streams undergo rapid fluctuations that are correlated, sometimes negatively, with the daily photocycle. The oscillations for particulate phases (turbidity, TSS, $Hg_{P.ngL}$, $MMHg_{P.ngL}$) were consistent within seasons, excluding the upstream industrial site, and were opposite in contrasting summer and winter seasons for some dissolved phases (e.g., $MMHg_D$ at the forested site). Both biotic (bioturbation, Hg methylation) and abiotic (photochemical reactions, shading, pH variations) factors exerted control over the observed patterns leading to loss of some diel oscillations in winter which had lower overall biotic activity. In addition to providing insight into Hg transformations in freshwater stream ecosystems, the diel oscillations have important implications with respect to sampling designs, site management, inter-site comparisons, and uptake and toxicity to biotic receptors. For example, predictions of Hg bioaccumulation factors are much better when high concentrations of $MMHg_D$ are included in models [82]. Armed with that information, one might design sampling plans for $MMHg_D$ to target mid to late afternoon and keep sample timing consistent to ensure accurate assessments of long-term trends. Given the potential importance of photochemical reactions on in-stream concentrations, changes in shading regime (e.g., logging, canopy loss due to insect infestations) would be expected to have consequent effects on MMHg concentration dynamics. At a minimum, stream shading regime is another factor to include in inter-site comparisons of stream ecosystems. [83]Finally, from the perspective of ecosystem remediation, given that much of the MMHg appears to originate from in-stream sources in this system, the relatively rapid response of MMHg concentration to in-stream conditions gives hope that targeted actions could lead to rapid improvements in water quality and, ultimately, in the health of biotic receptors in the ecosystem[84].

6. DATA AVAILABILITY STATEMENT

The data presented in the paper and supplemental information are publicly available at https://msfa.ornl.gov/data/pages/MCI548.html [doi.org/10.12769/1861075]. For additional information please contact the corresponding author.

7. CONFLICTS OF INTEREST

There are no conflicts of interest to declare.

8. ACKNOWLEDGEMENTS

This work was funded by the US Department of Energy, Office of Science, Biological and Environmental Research, Subsurface Biogeochemical Research, and is a product of the Science Focus Area (SFA) at ORNL. Additional funding was provided by the Oak Ridge Office of Environmental Management, URS | CH2M Oak Ridge LLC. The isotope(s) used in this research were supplied by the United States Department of Energy Office of Science by the Isotope Program in the Office of Nuclear Physics. Oak Ridge National Laboratory is managed by UT-Battelle, LLC for the U.S Department of Energy under contract no. DE-AC05-00OR22725.

9. TABLES

Table 1. Summary of main diel patterns observed

Parameter	Season	Location	Peak Concentration	Mechanism
$Hg_{P.ngL}$, $MMHg_{P.ngL}$, TSS, Turbidity	Summer	Midstream urban/suburban, Downstream forested	Night	Sediment resuspension by benthic macrobiota
Hg_D	Summer, Winter	Upstream industrial, Downstream forested	Day	Photochemical release from particles; decreased sorption with pH change
$MMHg_D$	Summer	Upstream industrial, Midstream urban/suburban, Downstream forested	Day	MMHg production in periphyton biofilms
	Winter	Downstream forested	Night	Photodemethylation during day outpaced slower Hg methylation in colder temperatures

10. FIGURE CAPTIONS

Figure 1. Map of East Fork Poplar Creek and sampling sites in this study. Creek flow is from EFK 23.4 to EFK 5.4. SW = surface water, PW = pore water.

Figure 2. Temperature (A), dissolved oxygen concentration (B), and pH (C) for the diel sampling campaigns. Data were collected every 15 minutes, but symbols shown for every tenth data point for clarity. Shaded portions indicate the period from sunset to sunrise.

Figure 3. Turbidity and particulate Hg and MMHg ($ng \cdot L^{-1}$) concentration for the diel sampling campaigns. (A)-(C) Su2015 campaign at EFK 23.4 and EFK 16.2, (D)-(F) Su2013, W2014, and Su2015 campaigns at EFK 5.4. Shaded portions indicate the period from sunset to sunrise, the broader shaded portion in panels (D)-(F) and other figures represents nighttime for the W2014 campaign. Asterisks to the right of data points indicate potential outliers. Turbidity was not measured at EFK 23.4 in summer 2015.

Figure 4. Total suspended solids (symbols and lines) for each sampling campaign and site. The solid line in each plot represents the concurrently measured turbidity. Turbidity was not measured at EFK 23.4 in Su2015. Shaded portions indicate the period from sunset to sunrise. Asterisks to the right of data points indicate potential outliers.

Figure 5. DOC and dissolved total Hg and MMHg concentration for each diel sampling campaign. (A)-(C) Su2015 campaign at EFK 23.4 and EFK 16.2, (D)-(F) Su2013, W2014, and Su2015 campaigns at EFK 5.4. Shaded portions indicate the period from sunset to sunrise. Open symbols indicate potential outliers.

Figure 6. Dissolved gaseous mercury (DGM) at EFK 5.4 for the Su2013 and W2014 sampling campaigns. Shaded portions indicate the period from sunset to sunrise.

Figure 7. Water temperature (solid line) and dissolved MMHg concentration (symbols and dashed lines) in samples collected in the morning versus the afternoon from August 2013 through February 2014.

Figure 8. Turbidity versus discharge hysteresis curve for EFK 5.4 during the Su2015 campaign. The curve proceeds in a counterclockwise direction from the start of sampling where turbidity remained constant while discharge increased. After sunset, turbidity increased while discharge did not change. Turbidity then remained steady at the higher value while discharge decreased. Shortly after sunrise, turbidity decreased while discharge remained constant, then remained constant while discharge increased. Asterisk to the right of symbol indicates potential outlier.

Figure 9. Representative turbidity patterns at EFK 5.4 for each season. Shaded portions indicate the period from sunset to sunrise. The broad turbidity peaks in autumn and winter coincided with precipitation driven high flow events.

11. REFERENCES

1. C. C. Fuller and J. A. J. N. Davis, Influence of coupling of sorption and photosynthetic processes on trace element cycles in natural waters, *Nature*, 1989, **340**, 52-54.
2. E. C. Volkmar, S. S. Henson, R. A. Dahlgren, A. T. O'Geen and E. E. Van Nieuwenhuyse, Diel patterns of algae and water quality constituents in the San Joaquin River, California, USA, *Chem. Geol.*, 2011, **283**, 56-67.
3. S. A. Nagorski, J. N. Moore, T. E. McKinnon and D. B. Smith, Geochemical response to variable streamflow conditions in contaminated and uncontaminated streams, *Water Resour. Res.*, 2003, **39**.
4. D. L. Naftz, J. R. Cederberg, D. P. Krabbenhoft, K. R. Beisner, J. Whitehead and J. Gardberg, Diurnal trends in methylmercury concentration in a wetland adjacent to Great Salt Lake, Utah, USA, *Chem. Geol.*, 2011, **283**, 78-86.
5. J. A. Fleck, G. Gill, B. A. Bergamaschi, T. E. C. Kraus, B. D. Downing and C. N. Alpers, Concurrent photolytic degradation of aqueous methylmercury and dissolved organic matter, *Science of The Total Environment*, 2014, **484**, 263-275.
6. M. J. Cohen, M. J. Kurz, J. B. Heffernan, J. B. Martin, R. L. Douglass, C. R. Foster and R. G. Thomas, Diel phosphorus variation and the stoichiometry of ecosystem metabolism in a large spring-fed river, *Ecological Monographs*, 2013, **83**, 155-176.
7. J. B. Heffernan and M. J. Cohen, Direct and indirect coupling of primary production and diel nitrate dynamics in a subtropical spring-fed river, *Limnology and Oceanography*, 2010, **55**, 677-688.
8. D. A. Nimick, C. H. Gammons and S. R. Parker, Diel biogeochemical processes and their effect on the aqueous chemistry of streams: A review, *Chemical Geology*, 2011, **283**, 3-17.
9. S. D. Siciliano, N. J. O'Driscoll, R. Tordon, J. Hill, S. Beauchamp and D. R. S. Lean, Abiotic production of methylmercury by solar radiation, *Environ. Sci. Technol.*, 2005, **39**, 1071-1077.
10. D. P. Krabbenhoft, J. P. Hurley, M. L. Olson and L. B. Cleckner, Diel variability of mercury phase and species distributions in the Florida Everglades, *Biogeochemistry*, 1998, **40**, 311-325.
11. P. Sellers, C. A. Kelly, J. W. M. Rudd and A. R. MacHutchon, Photodegradation of methylmercury in lakes, *Nature*, 1996, **380**, 694-697.
12. S. J. Klapstein and N. J. O'Driscoll, Methylmercury Biogeochemistry in Freshwater Ecosystems: A Review Focusing on DOM and Photodemethylation, *Bulletin of Environmental Contamination and Toxicology*, 2018, **100**, 14-25.
13. D. A. Nimick, B. R. McCleskey, C. H. Gammons, T. E. Cleasby and S. R. Parker, Diel mercury-concentration variations in streams affected by mining and geothermal discharge, *Sci. Tot. Environ.*, 2007, **373**, 344-355.
14. J. M. Loar, A. J. Stewart and J. G. Smith, Twenty-Five Years of Ecological Recovery of East Fork Poplar Creek: Review of Environmental Problems and Remedial Actions, *Environ. Manage.*, 2011, **47**, 1010-1020.
15. A. J. Stewart, J. G. Smith and J. M. Loar, Long-Term Water-Quality Changes in East Fork Poplar Creek, Tennessee: Background, Trends, and Potential Biological Consequences, *Environ. Manage.*, 2011, **47**, 1021-1032.
16. S. C. Brooks and G. R. Southworth, History of mercury use and environmental contamination at the Oak Ridge Y-12 Plant, *Environ. Poll.*, 2011, **159**, 219-228.
17. A. Riscassi, C. Miller and S. Brooks, Seasonal and flow-driven dynamics of particulate and dissolved mercury and methylmercury in a stream impacted by an industrial mercury source, *Environ. Toxicol. Chem.*, 2016, **35**, 1386-1400.
18. P. D. Parr and J. F. Hughes, *Oak Ridge Reservation: Physical Characteristics and Natural Resources. ORNL/TM-2006/110*, Oak Ridge National Laboratory, 2006.
19. P. J. Mulholland, G. R. Best, C. C. Coutant, G. M. Hornberger, J. L. Meyer, P. J. Robinson, J. R. Stenberg, R. E. Turner, F. VeraHerrera and R. G. Wetzel, Effects of climate change on freshwater ecosystems of the south-eastern United States and the Gulf Coast of Mexico, *Hydrol. Proc.*, 1997, **11**, 949-970.
20. A. Riscassi, C. L. Miller and S. C. Brooks, Impact of collection container material and holding times on sample integrity for mercury and methylmercury in water, *Limnology and Oceanography-Methods*, 2014, **12**, 407-420.
21. D. Kocman, S. C. Brooks, C. L. Miller and X. P. L. Yin, Evaluation of centrifugal ultrafilters for size fractionation of total mercury and methylmercury in freshwaters, *Environ. Chem.*, 2013, **10**, 323-332.

22. U. S. EPA, *Method 1631, Revision E: Mercury in Water by Oxidation, Purge and Trap, and Cold Vapor Atomic Fluorescence Spectrometry*, U. S. Environmental Protection Agency, EPA-821-R-02-019, 2002.
23. U. S. EPA, *Method 1630: Methyl Mercury in Water by Distillation, Aqueous Ethylation, Purge and Trap, and CVAFS*, U. S. Environmental Protection Agency, EPA-821-R-01-020, January 2001, 2001.
24. H. Hintelmann and N. Ogrinc, in *Biogeochemistry of Environmentally Important Trace Elements*, eds. Y. Cai and O. C. Braids, Amer Chemical Soc, Washington, 2003, vol. 835, pp. 321-338.
25. J. L. Weishaar, G. R. Aiken, B. A. Bergamaschi, M. S. Fram, R. Fujii and K. Mopper, Evaluation of specific ultraviolet absorbance as an indicator of the chemical composition and reactivity of dissolved organic carbon, *Environ. Sci. Technol.*, 2003, **37**, 4702-4708.
26. R Core Team, R: A Language and Environment for Statistical Computing.*Journal*, 2021.
27. S. Chatterjee, A New Coefficient of Correlation, *Journal of the American Statistical Association*, 2021, **116**, 2009-2022.
28. S. Holmes and S. Chatterjee, XICOR: Association Measurement Through Cross Rank Increments.*Journal*, 2020, **Version 0.3.3**, Version 0.3.3.
29. J. Ball, M. Babister, R. Nathan, W. Weeks, E. Weinmann, M. Retallick and I. Testoni, eds., *Australian Rainfall and Runoff: A Guide to Flood Estimation*, Commonwealth of Australia (Geoscience Australia), 2019.
30. U. Skyllberg, in *Environmental Chemistry and Toxicology of Mercury*, eds. G. Liu, Y. Cai and N. O'Driscoll, John Wiley and Sons, 2012, ch. 7, pp. 219-258.
31. G. Lui, Y. Li and Y. Cai, in *Environmental Chemistry and Toxicology of Mercury*, eds. G. Liu, Y. Cai and N. O'driscoll, John Wiley and Sons, 2012, ch. 11, pp. 367-388.
32. R. A. Lavoie, M. Amyot and J.-F. Lapierre, Global Meta-Analysis on the Relationship Between Mercury and Dissolved Organic Carbon in Freshwater Environments, *Journal of Geophysical Research: Biogeosciences*, 2019, **124**, 1508-1523.
33. G. Mierle and R. Ingram, The role of humic substances in the mobilization of mercury from watersheds, *Water Air Soil Poll.*, 1991, **56**, 349-357.
34. J. A. Dittman, J. B. Shanley, C. T. Driscoll, G. R. Aiken, A. T. Chalmers and J. E. Towse, Ultraviolet absorbance as a proxy for total dissolved mercury in streams, *Environ. Pollut.*, 2009, **157**, 1953-1956.
35. T. F. Waters, The Drift of Stream Insects, *Ann. Rev. Entomol.*, 1972, **17**, 253-272.
36. J. B. Wallace, J. Webster and T. Cuffney, Stream detritus dynamics: Regulation by invertebrate consumers, *Oecologia*, 1982, **53**, 197-200.
37. D. C. Richardson, L. A. Kaplan, J. Denis Newbold and A. K. Aufdenkampe, Temporal dynamics of seston: A recurring nighttime peak and seasonal shifts in composition in a stream ecosystem, *Limnology and Oceanography*, 2009, **54**, 344-354.
38. J. V. Loperfido, C. L. Just, A. N. Papanicolaou and J. L. Schnoor, In situ sensing to understand diel turbidity cycles, suspended solids, and nutrient transport in Clear Creek, Iowa, *Water Resour. Res.*, 2010, **46**, W06525.
39. C. M. Brick and J. N. Moore, Diel Variation of Trace Metals in the Upper Clark Fork River, Montana, *Environ. Sci. Technol.*, 1996, **30**, 1953-1960.
40. U. S. Department of Energy, *4. The Y-12 National Security Complex*, https://doeic.science.energy.gov/aser/aser2020/index.html, 2021.
41. M. J. Peterson, M. S. Greeley Jr., R. T. Jett, T. J. Mathews, S. C. Brooks, J. G. Smith, R. A. McManamay, N. J. Jones and N. Griffiths, *Y-12 National Security Complex Biological Monitoring and Abatement Program—2016 Calendar Year Report*, Oak Ridge National Laboratory, ORNL/SR-2017/331, 2017.
42. A. Johs, V. A. Eller, T. L. Mehlhorn, S. C. Brooks, D. P. Harper, M. A. Mayes, E. M. Pierce and M. J. Peterson, Dissolved organic matter reduces the effectiveness of sorbents for mercury removal, *Science of The Total Environment*, 2019, **690**, 410-416.
43. M. Haitzer, G. R. Aiken and J. N. Ryan, Binding of mercury(II) to dissolved organic matter: The role of the mercury-to-DOM concentration ratio, *Environ. Sci. Technol.*, 2002, **36**, 3564-3570.
44. M. Haitzer, G. R. Aiken and J. N. Ryan, Binding of mercury(II) to aquatic humic substances: Influence of pH and source of humic substances, *Environ. Sci. Technol.*, 2003, **37**, 2436-2441.
45. M. E. Brigham, D. A. Wentz, G. R. Aiken and D. P. Krabbenhoft, Mercury Cycling in Stream Ecosystems. 1. Water Column Chemistry and Transport, *Environ. Sci. Technol.*, 2009, **43**, 2720-2725.
46. D. A. Dzombak and F. M. M. Morel, *Surface Complexation Modeling: Hydrous Ferric Oxide*, John Wiley & Sons, New York, 1990.
47. W. M. Dong, L. Y. Liang, S. Brooks, G. Southworth and B. H. Gu, Roles of dissolved organic matter in the speciation of mercury and methylmercury in a contaminated ecosystem in Oak Ridge, Tennessee, *Environ. Chem.*, 2010, **7**, 94-102.

48. C. L. Miller, G. R. Southworth, S. C. Brooks, L. Liang and B. Gu, Kinetic controls on the complexation between mercury and dissolved organic matter in a contaminated environment, *Environ. Sci. Technol.*, 2009, **43**, 8548-8553.

49. G. M. M. Rahman and H. M. S. Kingston, Application of Speciated Isotope Dilution Mass Spectrometry To Evaluate Extraction Methods for Determining Mercury Speciation in Soils and Sediments, *Anal. Chem.*, 2004, **76**, 3548-3555.

50. T. D. Sowers, J. W. Stuckey and D. L. Sparks, The synergistic effect of calcium on organic carbon sequestration to ferrihydrite, *Geochemical Transactions*, 2018, **19**, 4.

51. M. L. Nguyen, W. C. Hockaday and B. L. T. Lau, Is the adsorption of soil organic matter to haematite (α-Fe_2O_3) temperature dependent?, *Eur J Soil Sci*, 2018, **69**, 892-901.

52. J. A. Fleck, B. D. Downing, J. F. Saraceno, G. Gill, M. Stephenson, C. N. Alpers and B. A. Bergamaschi, presented in part at the Geological Society of America Annual Meeting, 18-21 October 2009, Portland, OR, 2009.

53. C. C. Gilmour, M. Podar, A. L. Bullock, A. M. Graham, S. D. Brown, A. C. Somenahally, A. Johs, R. A. Hurt, K. L. Bailey and D. A. Elias, Mercury Methylation by Novel Microorganisms from New Environments, *Environmental Science & Technology*, 2013, **47**, 11810-11820.

54. J. M. Parks, A. Johs, M. Podar, R. Bridou, R. A. Hurt, S. D. Smith, S. J. Tomanicek, Y. Qian, S. D. Brown, C. C. Brandt, A. V. Palumbo, J. C. Smith, J. D. Wall, D. A. Elias and L. Liang, The Genetic Basis for Bacterial Mercury Methylation, *Science*, 2013, **339**, 1332-1335.

55. T. Barkay, S. M. Miller and A. O. Summers, Bacterial mercury resistance from atoms to ecosystems, *FEMS Microbiol. Rev.*, 2003, **27**, 355-384.

56. T. Barkay and B. Gu, Demethylation─The Other Side of the Mercury Methylation Coin: A Critical Review, *ACS Environmental Au*, 2021, DOI: 10.1021/acsenvironau.1c00022.

57. D. Achá, H. Hintelmann and J. Yee, Importance of sulfate reducing bacteria in mercury methylation and demethylation in periphyton from Bolivian Amazon region, *Chemosphere*, 2011, **82**, 911-916.

58. L. B. Cleckner, C. C. Gilmour, J. P. Hurley and D. P. Krabbenhoft, Mercury Methylation in Periphyton of the Florida Everglades, *Limnol. Oceanogr.*, 1999, **44**, 1815-1825.

59. M. Desrosiers, D. Planas and A. Mucci, Mercury Methylation in the Epilithon of Boreal Shield Aquatic Ecosystems, *Environmental Science & Technology*, 2006, **40**, 1540-1546.

60. S. Hamelin, M. Amyot, T. Barkay, Y. Wang and D. Planas, Methanogens: Principal Methylators of Mercury in Lake Periphyton, *Environ. Sci. Technol.*, 2011, **45**, 7693-7700.

61. C.-C. Lin and J. A. Jay, Mercury Methylation by Planktonic and Biofilm Cultures of *Desulfovibrio desulfuricans*, *Environmental Science & Technology*, 2007, **41**, 6691-6697.

62. J. B. Mauro, J. R. Guimarães, H. Hintelmann, C. J. Watras, E. A. Haack and S. A. Coelho-Souza, Mercury methylation in macrophytes, periphyton, and water -- comparative studies with stable and radio-mercury additions, *Anal Bioanal Chem*, 2002, **374**, 983-989.

63. L. Huguet, S. Castelle, J. Schäfer, G. Blanc, R. Maury-Brachet, C. Reynouard and F. Jorand, Mercury methylation rates of biofilm and plankton microorganisms from a hydroelectric reservoir in French Guiana, *The Science of the total environment*, 2010, **408**, 1338-1348.

64. W. L. Lazaro, S. Diez, C. J. da Silva, A. R. A. Ignacio and J. R. D. Guimaraes, Seasonal changes in peryphytic microbial metabolism determining mercury methylation in a tropical wetland, *Science of the Total Environment*, 2018, **627**, 1345-1352.

65. J. R. Guimarães, J. B. Mauro, M. Meili, M. Sundbom, A. L. Haglund, S. A. Coelho-Souza and L. D. Hylander, Simultaneous radioassays of bacterial production and mercury methylation in the periphyton of a tropical and a temperate wetland, *J Environ Manage*, 2006, **81**, 95-100.

66. T. A. Olsen, C. C. Brandt and S. C. Brooks, Periphyton Biofilms Influence Net Methylmercury Production in an Industrially Contaminated System, *Environ. Sci. Technol.*, 2016, **50**, 10843-10850.

67. G. E. Schwartz, T. A. Olsen, K. A. Muller and S. C. Brooks, Ecosystem Controls on Methylmercury Production by Periphyton Biofilms in a Contaminated Stream: Implications for Predictive Modeling, *Environ. Toxicol. Chem.*, 2019, **38**, 2426-2435.

68. C. C. Gilmour, D. A. Elias, A. M. Kucken, S. D. Brown, A. V. Palumbo, C. W. Schadt and J. D. Wall, Sulfate-Reducing Bacterium *Desulfovibrio desulfuricans* ND132 as a Model for Understanding Bacterial Mercury Methylation, *Appl. Environ. Microbiol.*, 2011, **77**, 3938-3951.

69. J. K. Schaefer, S. S. Rocks, W. Zheng, L. Y. Liang, B. H. Gu and F. M. M. Morel, Active transport, substrate specificity, and methylation of Hg(II) in anaerobic bacteria, *Proc. Natl. Acad. Sci. U. S. A.*, 2011, **108**, 8714-8719.

70. A. M. Graham, A. L. Bullock, A. C. Maizel, D. A. Elias and C. C. Gilmour, Detailed Assessment of the Kinetics of Hg-Cell Association, Hg Methylation, and Methylmercury Degradation in Several Desulfovibrio Species, *Appl. Environ. Microbiol.*, 2012, **78**, 7337-7346.
71. D. Zhang, Y. Yin, Y. Li, Y. Cai and J. Liu, Critical role of natural organic matter in photodegradation of methylmercury in water: Molecular weight and interactive effects with other environmental factors, *Science of The Total Environment*, 2017, **578**, 535-541.
72. Y. Qian, X. Yin, H. Lin, B. Rao, S. C. Brooks, L. Liang and B. Gu, Why Dissolved Organic Matter Enhances Photodegradation of Methylmercury, *Environmental Science & Technology Letters*, 2014, **1**, 426-431.
73. S. C. Brooks, C. L. Miller, A. L. Riscassi, K. A. Lowe, J. O. Dickson and G. E. Schwartz, Increasing temperature and flow management alter mercury dynamics in East Fork Poplar Creek, *Hydrological Processes*, 2021, **35**, e14344.
74. M. Amyot, G. Mierle, D. R. S. Lean and D. J. McQueen, Sunlight-induced formation of dissolved gaseous mercury in lake waters, *Environ. Sci. Technol.*, 1994, **28**, 2366-2371.
75. C. Dill, T. Kuiken, H. Zhang and M. Ensor, Diurnal variation of dissolved gaseous mercury (DGM) levels in a southern reservoir lake (Tennessee, USA) in relation to solar radiation, *Sci. Tot. Environ.*, 2006, **357**, 176-193.
76. E. Garcia, A. J. Poulain, M. Amyot and P. A. Ariya, Diel variations in photoinduced oxidation of Hg^0 in freshwater, *Chemosphere*, 2005, **59**, 977-981.
77. N. J. O'Driscoll, L. Poissant, J. Canario, J. Ridal and D. R. S. Lean, Continuous analysis of dissolved gaseous mercury and mercury volatilization in the upper St. Lawrence River: Exploring temporal relationships and UV attenuation, *Environ. Sci. Technol.*, 2007, **41**, 5342-5348.
78. S. D. Siciliano, N. J. O'Driscoll and D. R. S. Lean, Microbial reduction and oxidation of mercury in freshwater lakes, *Environ. Sci. Technol.*, 2002, **36**, 3064-3068.
79. H. Zhang, C. Dill, T. Kuiken, M. Ensor and W. C. Crocker, Change of dissolved gaseous mercury concentrations in a southern reservoir lake (Tennessee) following seasonal variation of solar radiation, *Environ. Sci. Technol.*, 2006, **40**, 2114-2119.
80. J. D. Demers, J. D. Blum, S. C. Brooks, Patrick M. Donovan, A. L. Riscassi, C. L. Miller, W. Zheng and B. Gu, Hg isotopes reveal in-stream processing and legacy inputs in East Fork Poplar Creek, Oak Ridge, Tennessee, USA, *Environmental Science: Processes & Impacts*, 2018, **20**, 686-707.
81. A. C. Maprani, T. A. Al, K. T. MacQuarrie, J. A. Dalziel, S. A. Shaw and P. A. Yeats, Determination of Mercury Evasion in a Contaminated Headwater Stream, *Environ. Sci. Technol.*, 2005, **39**, 1679-1687.
82. K. Riva-Murray, P. M. Bradley, B. C. Scudder Eikenberry, C. D. Knightes, C. A. Journey, M. E. Brigham and D. T. Button, Optimizing Stream Water Mercury Sampling for Calculation of Fish Bioaccumulation Factors, *Environ. Sci. Technol.*, 2013, **47**, 5904-5912.
83. D. A. Nimick, D. D. Harper, A. M. Farag, T. E. Cleasby, E. MacConnell and D. Skaar, Influence of in-stream diel concentration cycles of dissolved trace metals on acute toxicity to one-year-old cutthroat trout (*Oncorhynchus clarki lewisi*), *Environ. Toxicol. Chem.*, 2007, **26**, 2667-2678.
84. P. J. Blanchfield, J. W. M. Rudd, L. E. Hrenchuk, M. Amyot, C. L. Babiarz, K. G. Beaty, R. A. D. Bodaly, B. A. Branfireun, C. C. Gilmour, J. A. Graydon, B. D. Hall, R. C. Harris, A. Heyes, H. Hintelmann, J. P. Hurley, C. A. Kelly, D. P. Krabbenhoft, S. E. Lindberg, R. P. Mason, M. J. Paterson, C. L. Podemski, K. A. Sandilands, G. R. Southworth, V. L. St Louis, L. S. Tate and M. T. Tate, Experimental evidence for recovery of mercury-contaminated fish populations, *Nature*, 2022, **601**, 74-78.

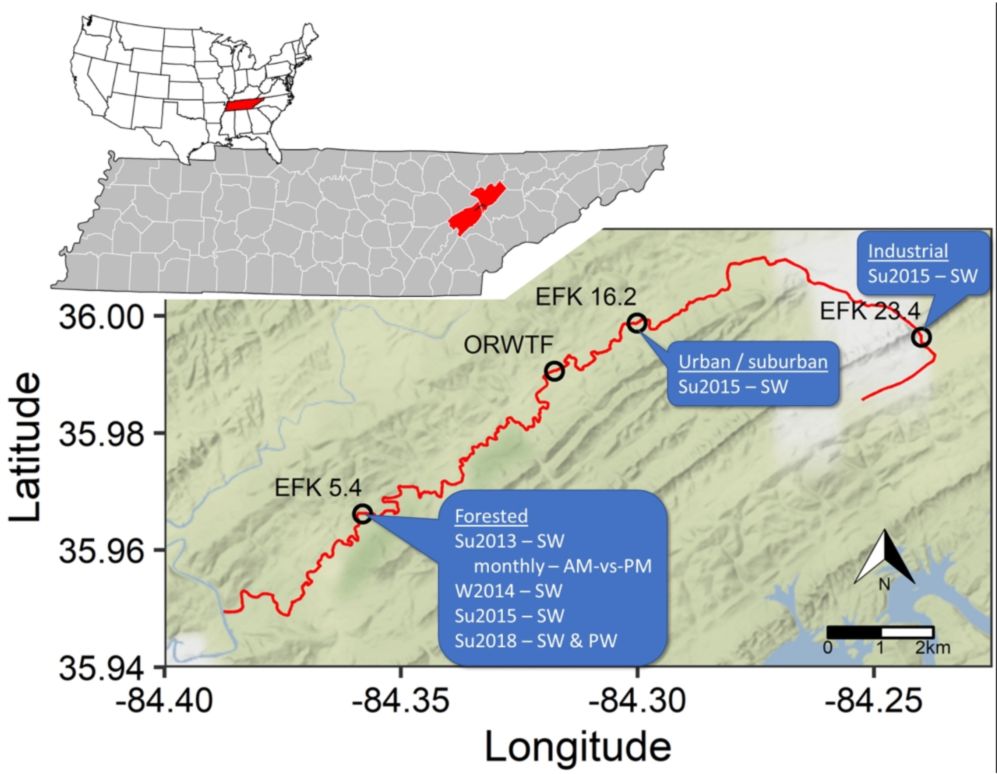

Figure 1. Map of East Fork Poplar Creek and sampling sites in this study. Creek flow is from EFK 23.4 to EFK 5.4. SW = surface water, PW = pore water.

1817x1400mm (28 x 28 DPI)

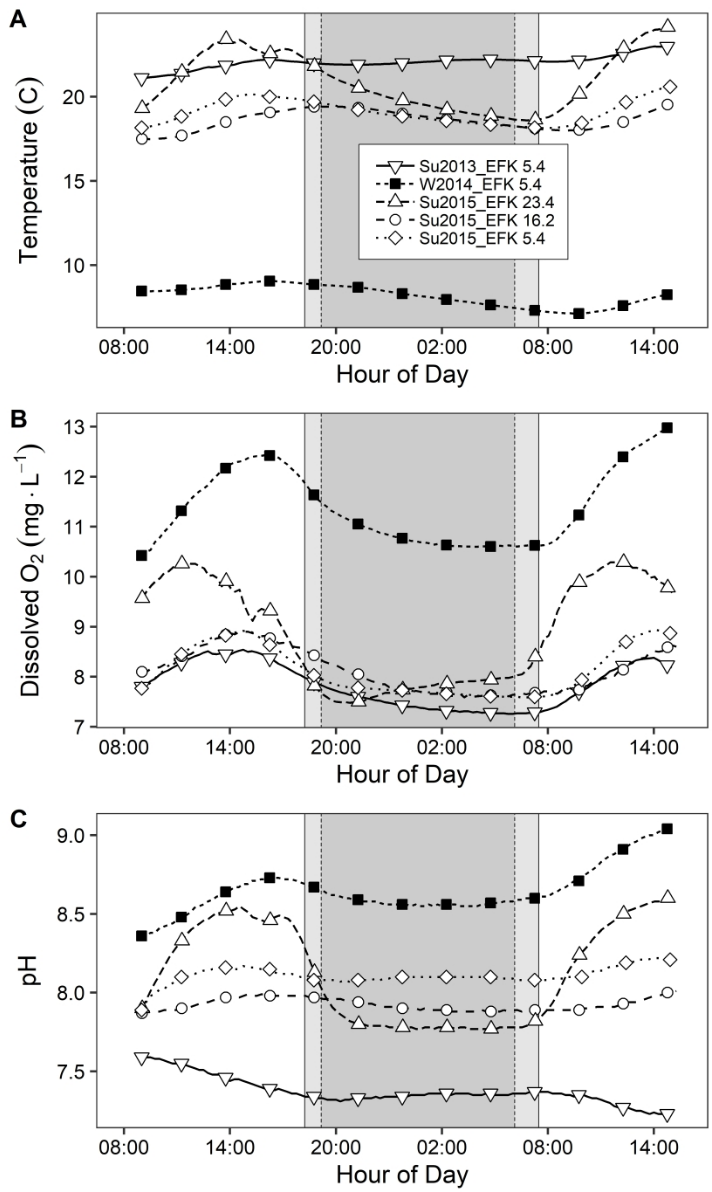

Figure 2. Temperature (A), dissolved oxygen concentration (B), and pH (C) for the diel sampling campaigns. Data were collected every 15 minutes, but symbols shown for every tenth data point for clarity. Shaded portions indicate the period from sunset to sunrise.

774x1290mm (126 x 126 DPI)

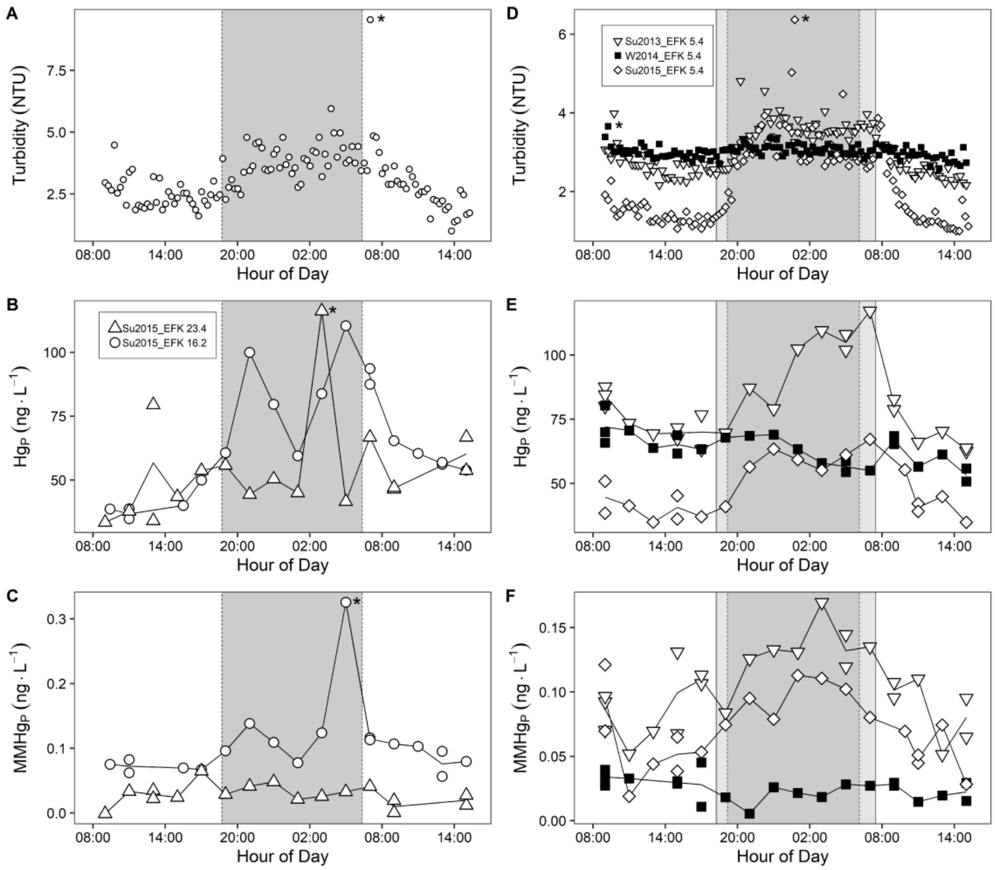

Figure 3. Turbidity and particulate Hg and MMHg ($ng{\cdot}L^{-1}$) concentration for the diel sampling campaigns. (A)-(C) Su2015 campaign at EFK 23.4 and EFK 16.2, (D)-(F) Su2013, W2014, and Su2015 campaigns at EFK 5.4. Shaded portions indicate the period from sunset to sunrise, the broader shaded portion in panels (D)-(F) and other figures represents nighttime for the W2014 campaign. Asterisks to the right of data points indicate potential outliers. Turbidity was not measured at EFK 23.4 in summer 2015.

1362x1192mm (126 x 126 DPI)

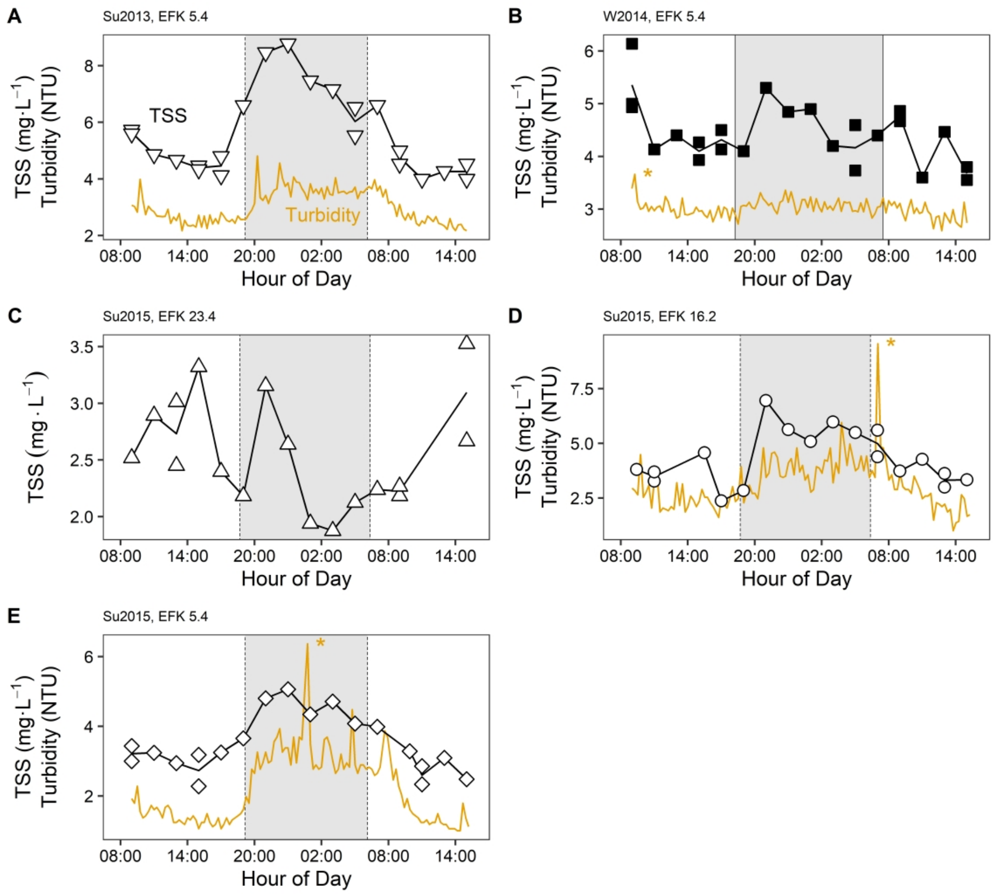

Figure 4. Total suspended solids (symbols and lines) for each sampling campaign and site. The solid line in each plot represents the concurrently measured turbidity. Turbidity was not measured at EFK 23.4 in Su2015. Shaded portions indicate the period from sunset to sunrise. Asterisks to the right of data points indicate potential outliers.

1290x1161mm (126 x 126 DPI)

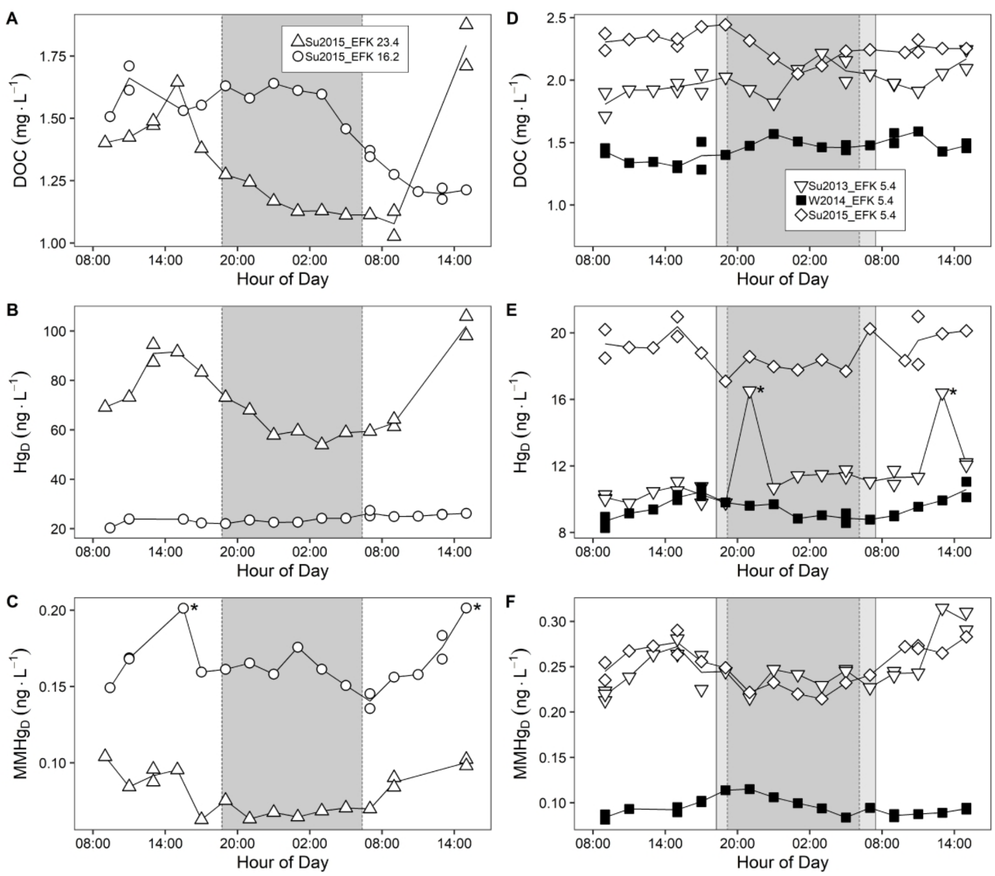

Figure 5. DOC and dissolved total Hg and MMHg concentration for each diel sampling campaign. (A)-(C) Su2015 campaign at EFK 23.4 and EFK 16.2, (D)-(F) Su2013, W2014, and Su2015 campaigns at EFK 5.4. Shaded portions indicate the period from sunset to sunrise. Open symbols indicate potential outliers.

1362x1192mm (126 x 126 DPI)

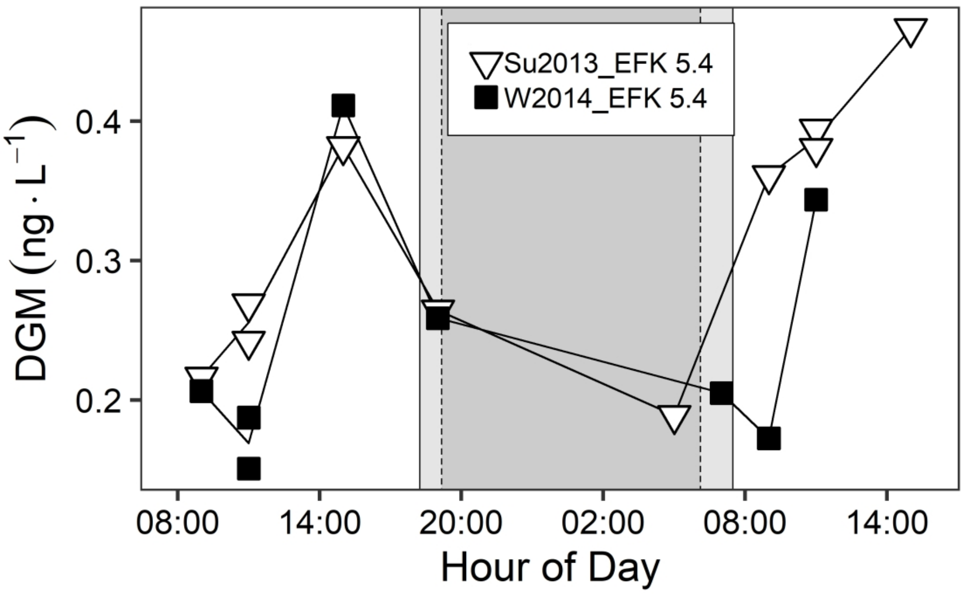

Figure 6. Dissolved gaseous mercury (DGM) at EFK 5.4 for the Su2013 and W2014 sampling campaigns. Shaded portions indicate the period from sunset to sunrise.

645x403mm (126 x 126 DPI)

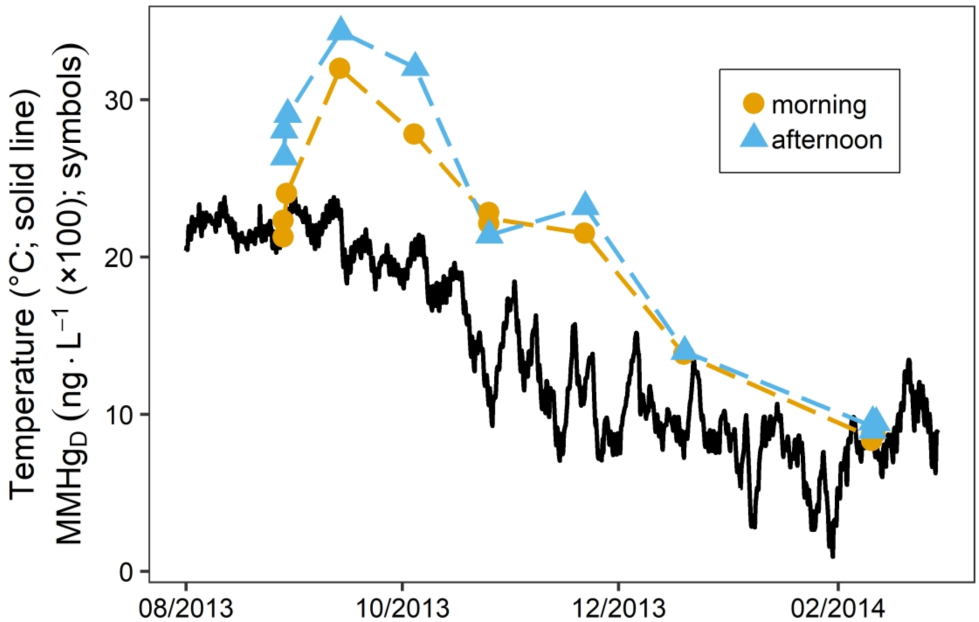

Figure 7. Water temperature (solid line) and dissolved MMHg concentration (symbols and dashed lines) in samples collected in the morning versus the afternoon from August 2013 through February 2014.

645x419mm (126 x 126 DPI)

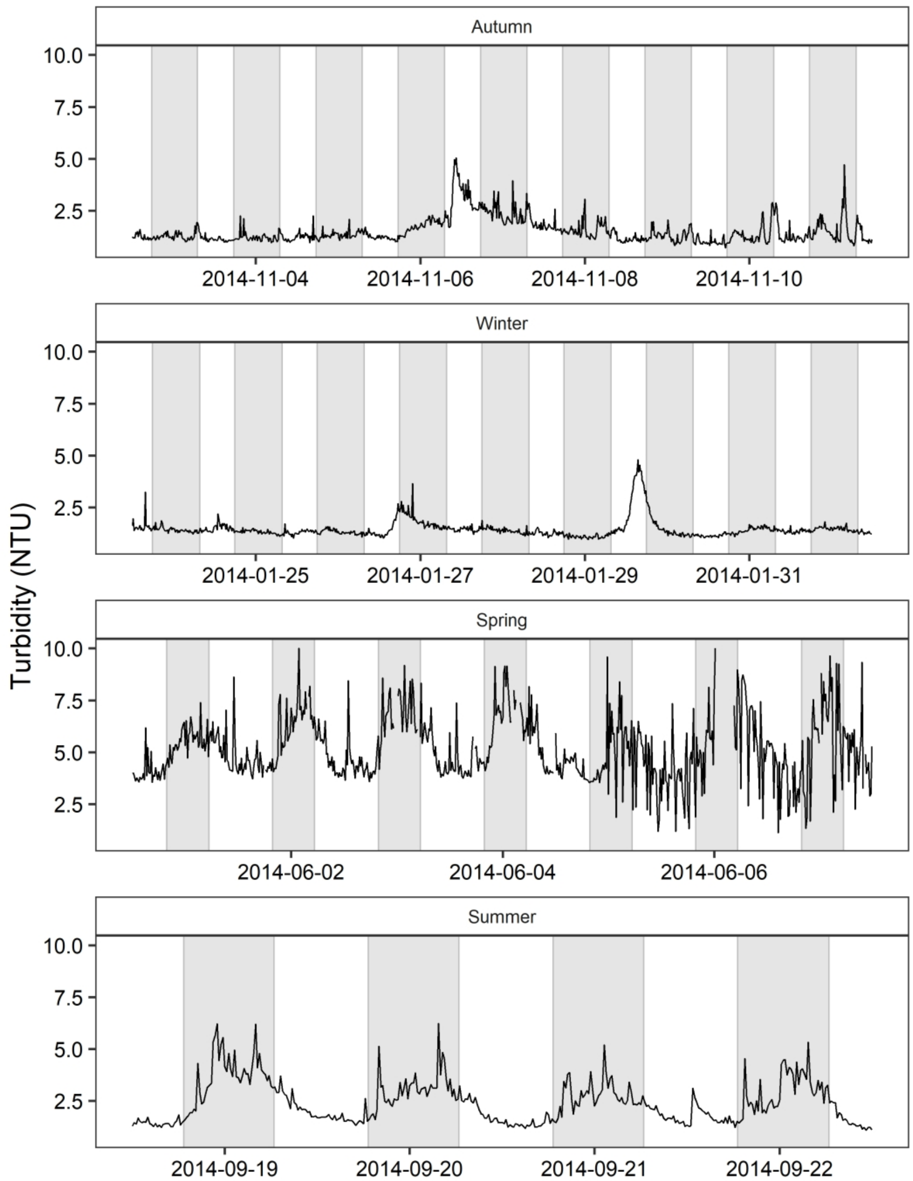

Figure 8. Representative turbidity patterns at EFK 5.4 for each season. Shaded portions indicate the period from sunset to sunrise. The broad turbidity peaks in autumn and winter coincided with precipitation driven high flow events.

548x709mm (126 x 126 DPI)

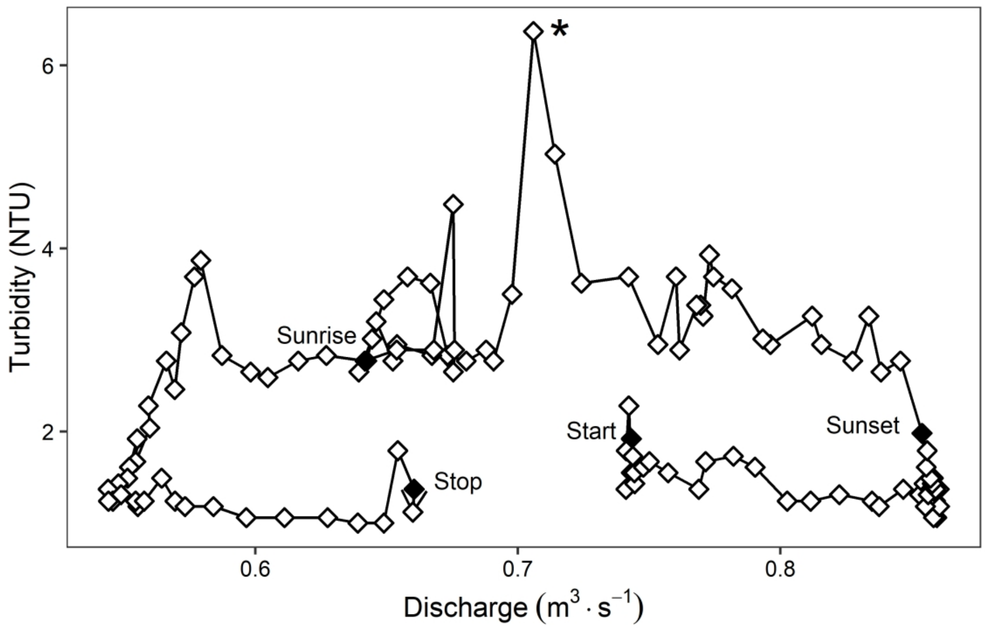

Figure 9. Turbidity versus discharge hysteresis curve for EFK 5.4 during the Su2015 campaign. The curve proceeds in a counterclockwise direction from the start of sampling where turbidity remained constant while discharge increased. After sunset, turbidity increased while discharge did not change. Turbidity then remained steady at the higher value while discharge decreased. Shortly after sunrise, turbidity decreased while discharge remained constant, then remained constant while discharge increased. Asterisk to the right of symbol indicates potential outlier.

645x419mm (126 x 126 DPI)